Biophysical Journal, Volume *119*

Supplemental Information

Fusion Pore Formation Observed during SNARE-Mediated Vesicle Fusion with Pore-Spanning Membranes

Peter Mühlenbrock, Kira Herwig, Loan Vuong, Ingo Mey, and Claudia Steinem

1. Encapsulation of sulforhodamine B into vesicles and bulk vesicle fusion assay

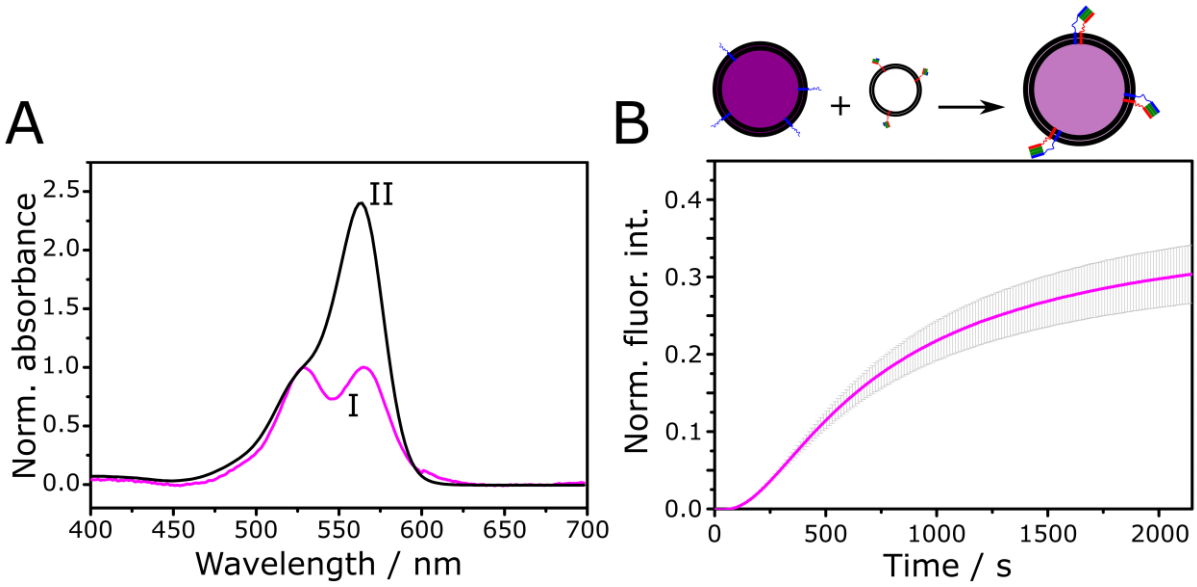

FIGURE S1 (A) Normalized absorbance spectra of (I) encapsulated and (II) free sulforhodamine B. (B) Bulk fusion assay to verify the fusion activity of reconstituted SNAREs prior to the single vesicle experiments with pore-spanning membranes.

Successfull encapsulation of sulforhodamine B (SRB, 43 mM) into proteoliposomes was analyzed by measuring absorbance spectra of the vesicle suspension in buffer B (20 mM HEPES, 121 mM KCl, 1 mM dithiothreitol, pH 7.4, 255 mOsmol/L) (Fig. S1A, I). At 43 mM, SRB is concentration quenched and exhibits two absorption maxima with almost equal intensities. Adding Triton X-100 to the suspension leads to vesicle lysis and an increase of the absorption maximum at around 560 nm (Fig. S1A, II). This change in the absorbance spectrum is due to dimerization of SRB at high concentrations (1).

Functional protein reconstitution was investigated using a bulk content release assay. Synaptobrevin 2 containing large unilamellar vesicles (LUVs) were fused with ΔN49 complex containing small unilamellar vesicles (SUVs) (Fig. S1B). LUVs (10 nmol lipid) were mixed with SUVs (10 nmol lipid) in a total volume of 750 µL adjusted with buffer B. Time-dependent fluorescence dequenching of SRB upon fusion of the vesicles was monitored. SRB fluorescence was excited at λ_{ex} = 560 nm and fluorescence emission was recorded at λ_{em} = 590 nm at T = 22 °C. Triton X-100 was added as an internal standard for full dye dequenching.

2. Reconstitution efficiency of the fusion active acceptor complex

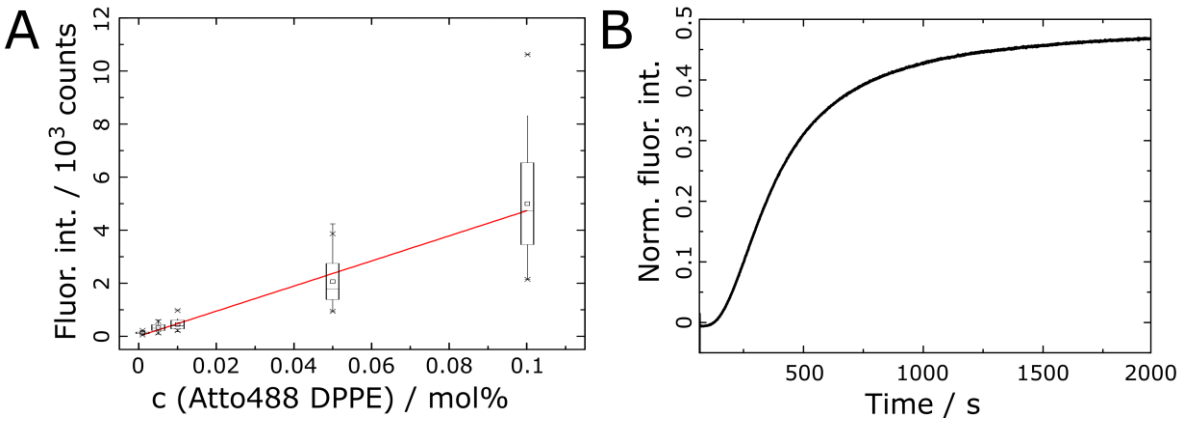

FIGURE S2 (A) Calibration curve to determine the reconstitution efficiency *R* of the ΔN49 complex in GUVs. A slope M_{ref} = 47,300 counts/mol% was obtained from a weigthened linear regression (*N* = 98). (B) Bulk content release assay to analyze the fusion activity of the Atto488-labeled ΔN49-complex reconstituted in SUVs and fused with SRB-loaded synaptobrevin containing LUVs.

3. Finite element simulations of indirect FRAP experiments

To determine diffusion coefficients of lipids and proteins in the s-PSM, recovery curves of indirect FRAP experiments were compared with simulated recovery curves. Finite element simulations (FEM, COMSOL Multiphysics v4.4) were carried out assuming

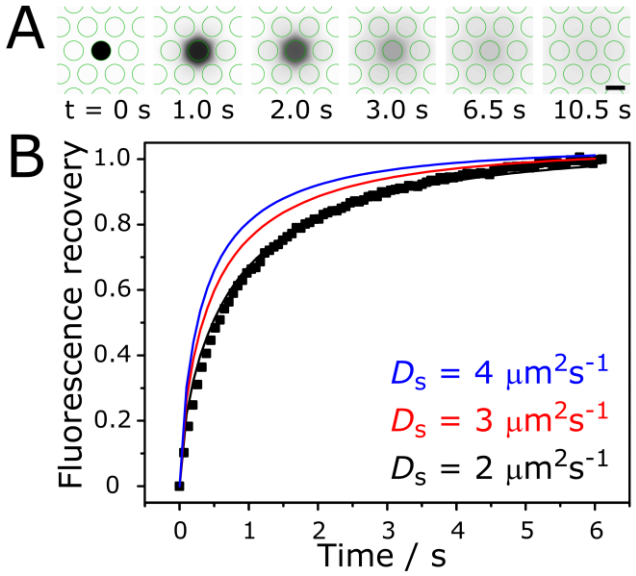

FIGURE S3 (A) Simulated images of a fluorescence recovery over time; scale bar: 5 µm. (B) Averaged (*N* = 33) and normalized, time dependent fluorescence recovery curve obtained from an Atto390 DPPE labeled pore-spanning membrane composed of DOPC/POPE/POPS/cholesterol (5:2:1:2, *n*/*n*) (black squares) and simulated recovery curves with D_{Lipid} (s-PSM) = 2 (black), 3 (red), and 4 µm² s^{-1} (blue) and D_{Lipid} (f-PSM) = 7.7 µm² s^{-1}.

different diffusion coefficients for the s- and f-PSM, respectively to solve Fick's second law (2):

$$\frac{\partial c_{\mathrm{i}}}{\partial t} = D_{\mathrm{i}} \nabla^2 c_{\mathrm{i}} \qquad \text{(S1)}$$

with c_i the surface concentration, t the time and D_i the diffusion coefficient. The diffusion coefficient of the lipids and proteins in the f-PSM was set to D_{Lipid} (f-PSM) = 7.7 μm^2 s^{-1} and $D_{\Delta N49}$ = 3.4 μm^2 s^{-1} as determined previously by means of FCS measurements (3). The substrate surface was modeled by a 60 × 60 μm^2 square with a hexagonal pore pattern with d_{pore} = 5 μm and a porosity of 36 % (Fig. S3A). As described by Höök et al. (2), an artificial bleach spot was placed in the center of the pore with radius 2.2 μm assuming a Gaussian intensity profile (Fig. S3A, t = 0 s) with the concentration $c_{\mathrm{r},0}$:

$$c_{\mathrm{r},0} = c_{\mathrm{eq}} \exp\left(-K \exp\left(\frac{-r^2}{w^2}\right)\right), \qquad \text{(S2)}$$

where c_{eq} = 1, w = 2.2 μm and K = 2. Theoretical fluorescence recovery images were monitored as depicted in Fig. S3A. Changing the diffusion coefficients for the protein and the lipid lead to the recovery curves as shown in Fig. 2C and Fig. S3B, respectively. A best fit between experimental data and simulated curve was found for a diffusion coefficient of $D_{\Delta N49}$ (s-PSM) = 1.0 ± 0.5 μm^2 s^{-1} and D_{Lipid} (s-PSM) = 2 ± 1 μm^2 s^{-1} with the error equal to the simulation step size.

4. Flow chart of the MATLAB routine to evaluate single vesicle fusion events

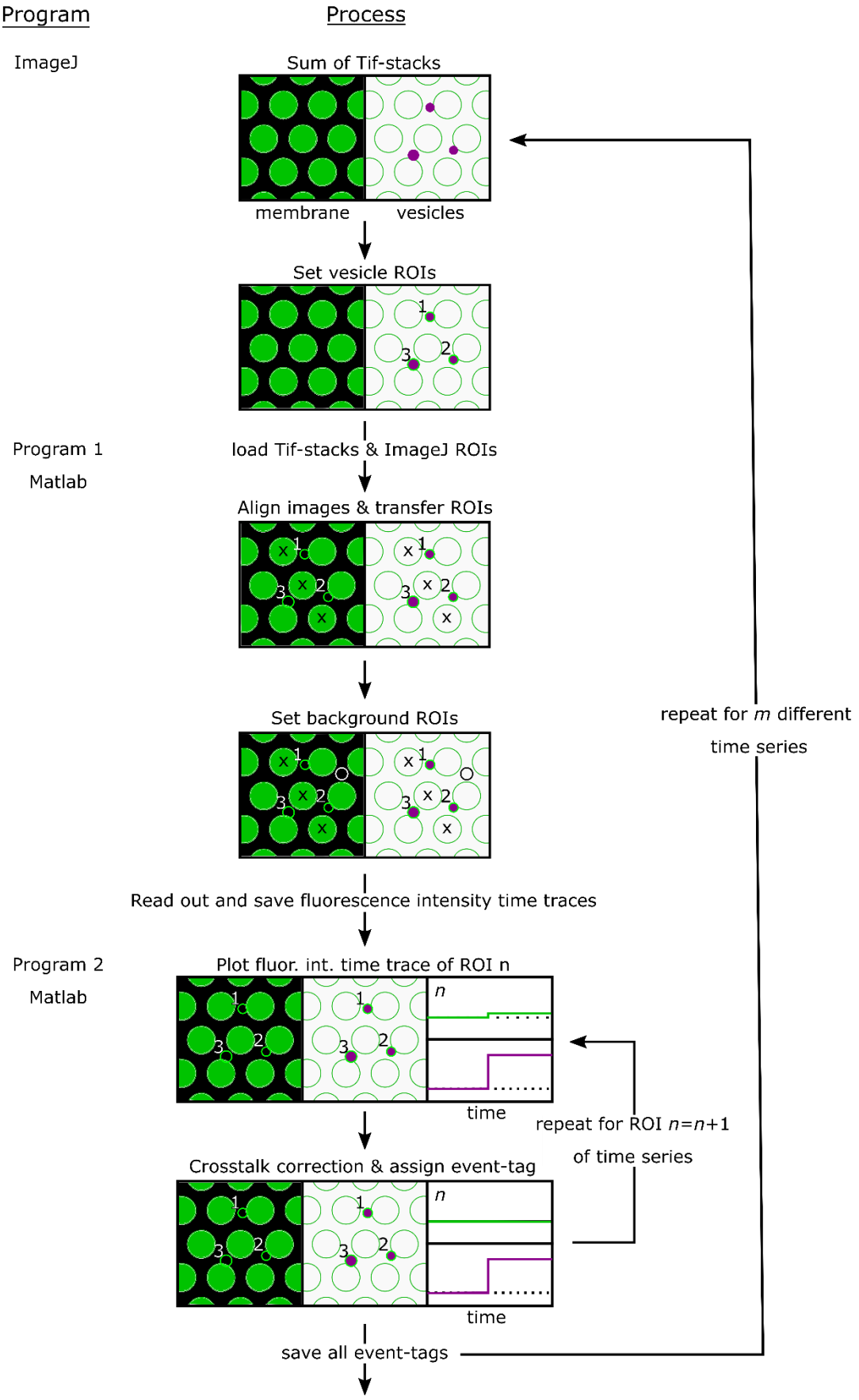

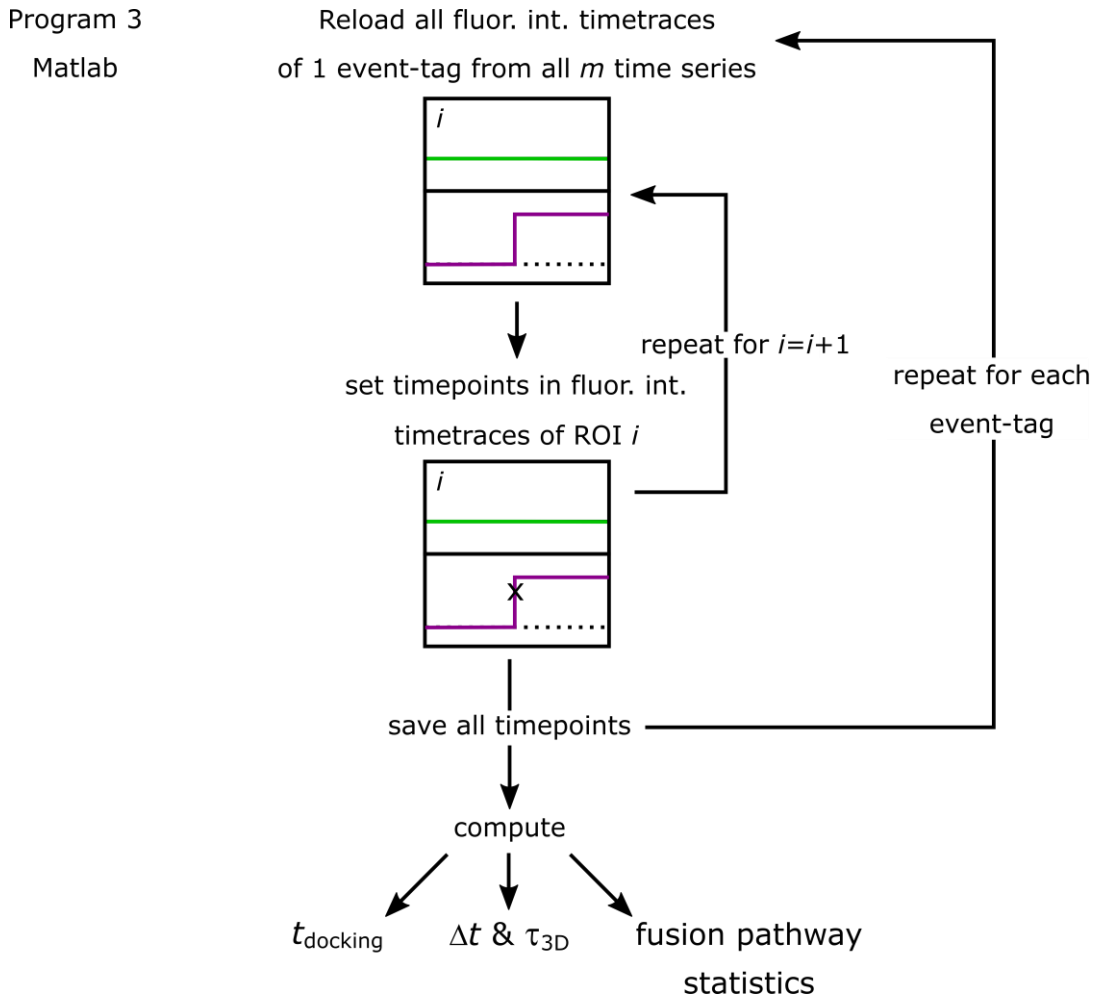

FIGURE S4 Process chart for the analysis of single vesicle fusion events. Each docked vesicle is tagged with a ROI using ImageJ. ROIs and Tif-stacks are loaded into program 1. Vesicle and membrane channels are aligned, a background ROI is set and fluorescence intensity time traces of each individual ROI pair are read out. Data is loaded into program 2, fluorescence crosstalk is corrected and event-tags are assigned to all *n* ROIs. This process is repeated for *m* different time series (Tif-stacks). Collective data of individual event-tags is loaded into program 3 and important time points for further calculations are set and extracted from the fluorescence intensity time traces.

Single vesicle fluorescence intensity time traces recorded by means of dual color fluorescence microscopy were evaluated individually using a custom-made MATLAB-script. A process chart to illustrate the procedures is given in Fig. S4. The programs can be found at: https://github.com/imey78/FusionAnalysis.git. To record the fluorescence intensities of the target membrane (Atto655 DPPE, false colored in green) and the vesicular content (sulforhodamine B (SRB), false colored in magenta) simultaneously, the two emission lines were separated and guided to each one half of the camera (split image). Due to large data amounts one time series consists of up to 6 Tif-stacks. Tif-stacks were loaded into ImageJ, the sum was created and each vesicle was tagged manually with a region of interest (ROI). Time series and ImageJ ROIs were loaded into program 1. To align the two channels, pore centers were selected on each site of the split image. ROIs were transferred and a ROI for dynamic background correction was set. Fluorescence intensity time traces of each ROI pair was read out

and saved. Data was reloaded into program 2 and fluorescence intensity time traces of each ROI *n* were displayed. To correct for the cross talk of the SRB fluorescence intensity into the Atto655 DPPE channel, SRB filled vesicles were immobilized on an empty substrate, imaged and a fluorescence intensity time trace was recorded under the same experimental conditions. The sum of the time series was created, ROIs on each side (left: *l*, right: *r*) of the split image were set and background ($BG_{l,r}$) corrected maximum fluorescence intensities (I_{max}) were read out. The correction factor (*CF*) was then calculated using eq. S3:

$$CF = \frac{1}{n}\sum_{i=1}^{n}\frac{(I_{\mathrm{max,l,i}}-BG_{\mathrm{l}})}{(I_{\mathrm{max,r,i}}-BG_{\mathrm{r}})} \qquad \text{(S3)}$$

After crosstalk correction an event-type was assigned to each individual ROI *n* (e.g. docked vesicle without fusion, Fig. S4), all event-tags were saved and the whole process was repeated for all *m* different time-series. All *i* fluorescence intensity time traces of one specific event-tag were loaded into program 3, plotted and time points of interest set. Respective time points were extracted, saved and used for further calculations.

5. Observation of a vesicle burst

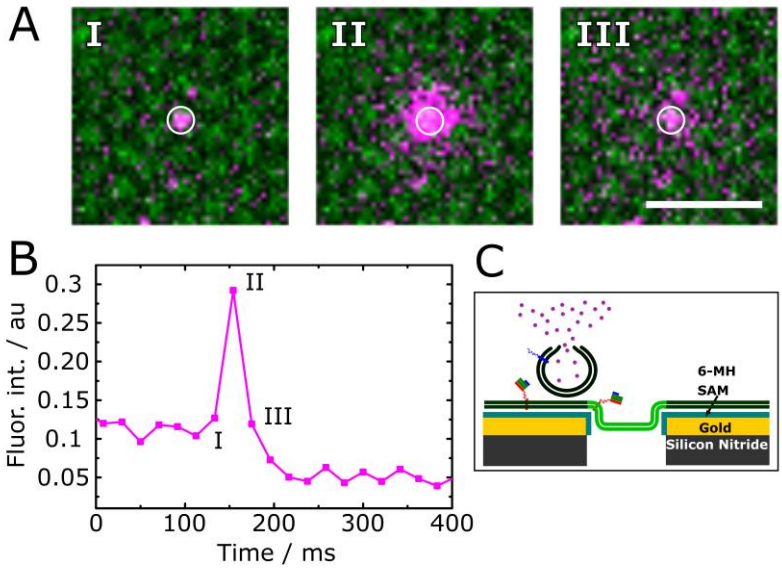

FIGURE S5 (A) Time lapse fluorescence images of a bursting vesicle (magenta); scale bar: 5 µm. (B) Fluorescence intensity time trace of the vesicle obtained from the region of interest shown in (A). After docking of the vesicle (I), the vesicle bursts resulting in a sharp spike in the SRB fluorescence intensity time trace (II), which then disappears (III) upon rapid diffusion of the dye into the bulk solution above the PSM. (C) Schematic illustration (not to scale) of a vesicle docked to the edge of the aqueous compartment and releasing its content into the bulk solution above the membrane.

6. Docking time distribution

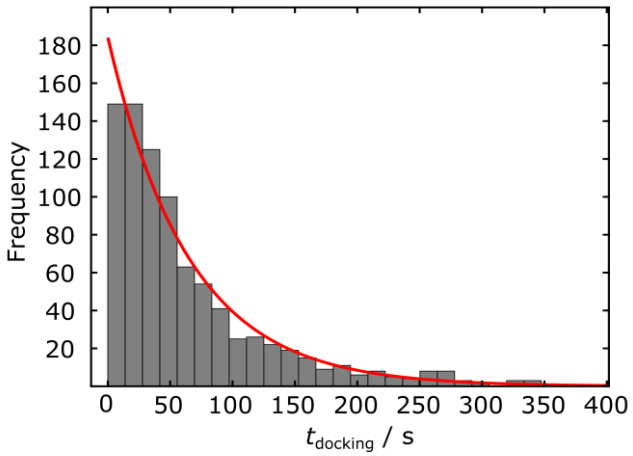

FIGURE S6 Docking time distribution obtained by extracting $t_{docking}$ from N = 840 fusion events. A mono-exponential decay function (red) was fit to the data with an average lifetime $\tau_{docking}$ = 65 ± 4 s.

7. Illustration of the fluorescent time traces

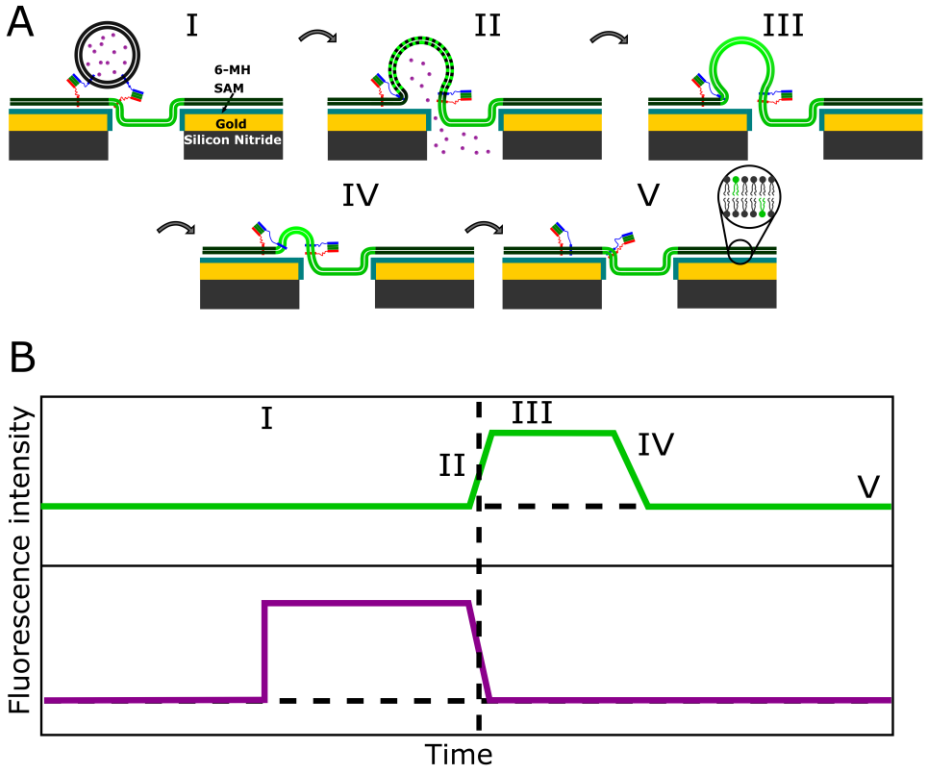

FIGURE S7 (A) Schematic illustration and (B) respective schematic fluorescence intensity time traces (both not to scale) of a vesicle fusing with the s-PSM with visible lipid mixing. When the vesicle docks to the membrane, the fluorescence intensity increases (magenta, I) while the fluorescence of the target membrane (green) is quenched due to the close proximity to the underlying gold surface. Upon fusion (II) the vesicle fluorescence intensity decreases due to the release of fluorophores into the aqueous compartment next to the s-PSM. Meanwhile lipids diffuse from the target membrane into the 3D structure of the vesicle. The distance of lipid fluorophores to the gold surface increases thus leading to an increase in fluorescence intensity (II) until the maximum is reached (III). The collapse of the vesicle into the target membrane results in a decrease in this fluorescence intensity (IV) till it is distributed and all fluorescence intensity is again quenched (V).

8. Comparison of docked vesicles with characteristic parameters of the fusion process

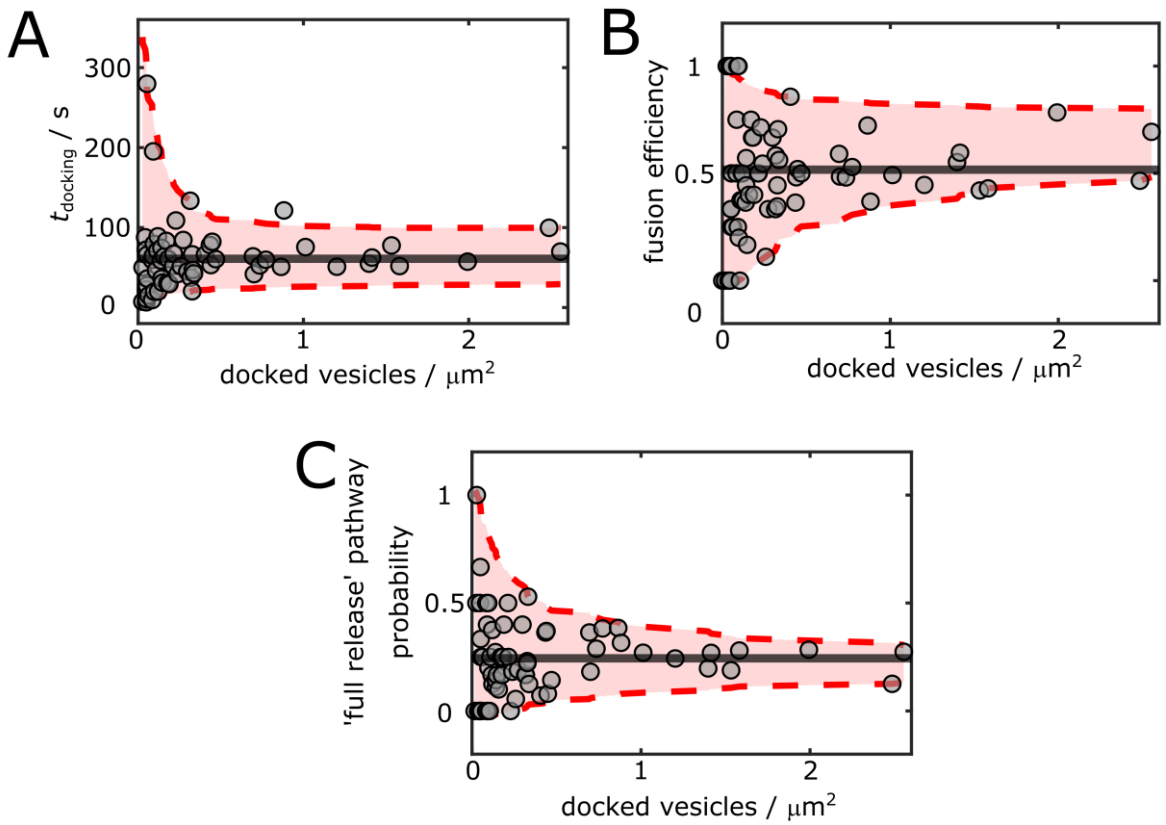

FIGURE S8 Scatter plots of the number of docked vesicles of individual membrane patches reflecting the active ΔN49 complexes in the f-PSMs with (A) the mean docking time, (B) the fusion efficiency and (C) the relative occurrence of the fusion pathway defined as 'full release' quantified for each individual membrane patch. Each population converges to its global mean value (grey horizontal line) with increasing number of docked vesicles as expected if no linear relationship is present. The calculated correlation coefficients R = 0.137 (A), 0.0584 (B), and 0.0355 (C) support this observation.

9. Fusion pathway statistics

TABLE S1 Total number N of events undergoing a certain fusion pathway used to calculate the mean values in Figure 7.

Fusion pathway	***N***
Full release	393
Incomplete release	202
Full release & vesicle collapse	107
Stable 3D postfusion structure	138
Bursting vesicle	6
No fusion pore formation	763

10. Supporting references

1. Chen, R. F., and J. R. Knutson. 1988. Mechanism of fluorescence concentration quenching of carboxyfluorescein in liposomes. Energy transfer to nonfluorescent dimers. *Anal. Biochem.* 172:61–77.
2. Jönsson, P., M. P. Jonsson, J. O. Tegenfeldt, and F. Höök. 2008. A method improving the accuracy of fluorescence recovery after photobleaching analysis. *Biophys. J.* 95:5334–5348.
3. Schwenen, L. L. G., R. Hubrich, D. Milovanovic, B. Geil, J. Yang, A. Kros, R. Jahn, and C. Steinem. 2015. Resolving single membrane fusion events on planar pore-spanning membranes. *Sci. Rep.* 5:12006.